PII: S0955-2219(98)00138-1

0955-2219/98/$—see front matter

Sorption and Gas Sensitive Properties of In_2O_3 Based Ceramics Doped with Ga_2O_3

A. Ratko,[a] O. Babushkin,[b]* A. Baran[a] and S. Baran[c]

[a]Institute of General and Inorganic Chemistry, Minsk, 220072 Belarus
[b]Division of Materials Science, Luleå University of Technology, S-951 87, Luleå, Sweden
[c]Pharmec Ltd, Minsk, Belarus

(Received 21 January 1998; accepted 3 June 1998)

Abstract

The process of structure formation in In_2O_3 based ceramics doped with Ga_2O_3 was investigated. The data obtained demonstrated the profound influence of Ga-dopands both on the crystallization path of solids produced by coprecipitation and on their final physical and electrical properties. The limited solubility of Ga_2O_3 dopands in cubic In_2O_3 lattice which lies within the 11–12 wt% was also noted. Ga_2O_3-dopands caused the formation of a porous structure in the In_2O_3-based ceramics, providing an active interaction surface in the semiconductor for reducing gases. Ga-doped ceramics demonstrated better gas sensor properties then pure In_2O_3.

1 Introduction

It is a well known fact that the improvement of the properties a gas sensors based on semiconductive metal oxides can be successfully achieved by sintering new materials or by modification of known types of sensors.

It was shown that there is a possibility of improvement of sensor properties such as sensitivity and selectivity with respect to analyzing gases, at the stage of sensors sintering. As mentioned in Ref. 1 the application of inorganic dopands added during sintering of gas sensors can improve selective adsorption. For instance, application of Al_2O_3 (4 wt%) in a ceramic based on In_2O_3 lead to increase sensor sensitivity with respect to reducing gases.[2]

The purpose of the present work is to investigate the structure, phase composition and sensitivity properties of In_2O_3 ceramics doped with Ga_2O_3. Selecting Ga_2O_3 as a dopand was due to the fact that both oxides are n-type semiconductors (for instance for Ga_2O_3 $E = 4{\cdot}6$–$4{\cdot}7$ eV) and Ga_2O_3 can be used for sintering gas sensors both for reducing gases as well oxygen.[3,4]

*To whom correspondence should be addressed. Fax: +46-920-993-09; e-mail:oleg.babushkin@mb.luth.se

2 Experimental procedure

2.1 Subject investigation

In-Ga-solids have been prepared via the coprecipitation route. Metal nitrates $In(NO_3)_3{\cdot}4{\cdot}5H_2O$ and $Ga(NO_3)_3{\cdot}8H_2O$ were dissolved in distilled water and diluted to 10% solution. Precipitation was performed with 12·5% NH_4 water solution at pH 8 forcing the precipitation of metal hydroxides. The precipitates were aged for 1 h and then washed in distilled water and sedimented by centrifuging. The content of the Ga_2O_3 in the precipitates was changed from 0 to 100 wt%. The precipitates were calcined at 120, 500, 700, 800 and 1000°C.

2.2 Differential thermal analysis

Differential thermal analysis of the precipitates were performed using a 'Derivatograph-Q 1500D' in conjunction with a thermogravimetric analyzer. The measurements (0·5 g) were done using Pt crucibles, in air, at a heating rate of 5°C min^{-1}. Calcined Al_2O_3 was used as a reference sample. Sensitivity for all measurements was selected 250 μV.

2.3 X-Ray diffraction examinations

The phase compositions developed during calcination were investigated by powder X–ray diffractometry in a Philips PW-1710 automatic diffractometer with step and continuous scanning device. The diffractometer was equipped with a vertical goniometer PW 1050/25, graphite

mono-chromator PW 1752/00, proportional counter for reflected beam PW 1711/10, and a PW 1730/25 generator. Diffraction patterns were measured in a 2Θ range of 10–90 using Cu K_α radiation of 50 kV and 30 mA. Accurate assignment of the peak positions was facilitated by fitting with a non-linear Marquardt least-squares routine that accounts for the K_α splitting. The lattice parameters of the In_2O_3–Ga_2O_3 solid solution formed were refined by application of a least-squares refinement program.

2.4 Surface area and porosimetry

Specific surface area (SSA) and pore analysis were conducted using a sorption analyzer with bensol as the adsorbate media. Adsorption of the bensol steam was done in a vacuum chamber equipped with a quartz Mac-Ben Bacra balance. For sorption measurements, samples (40–50 mg) in a glass container were placed in sorption tubes which were fixed on calibrated quartz spirals. Prior to analysis, the samples were degassed at 150°C for 4 h. Adsorption was measured at 20 ± 0·1°C. Adsorption–structural parameters were computed using Brunauer–Emmett–Teller (BET) and Tomson–Kelvin methods.

2.5 Electroconductivity measurements

Electroconductivity was measured by four-probe D.C. methods[5] in air and in air blended with 0·5 vol% methane. The samples used for measurements were shaped into a parallel block with dimensions 10×5×2 mm. The ceramic samples electroded with Pt were calcined at 800°C for one hour. Prior to measurements a heat-treatment at 600°C was carried out to degas the samples.

3 Results and Discussion

3.1 Differential thermal analysis

Thermogravimetric analysis indicated that the major portion of gel water for all investigated samples was eliminated when samples were heated to 400°C (Fig. 1). DTA studies were conducted to evaluate the correlation of crystallization events with appearance of powder patterns in the XRD studies and to determine the onset temperatures of crystallization more accurately. Results of DTA of the $In(OH)_3$ showed two endotherms. One was observed at 80–120°C and can be associated with the loss of absorbed water. The other was observed at 220–250°C and can be associated with the transition of hydroxide to oxide. With increasing $Ga(OH)_3$ content, the temperature of the second endotherm increased. For a precipitate with 20 wt% Ga-dopands the second endotherm increased to 268°C (Fig. 1) which is caused by the higher energy of Me–O bond for Ga^{3+} then for In^{3+}.[6] It is known that an energy increase of Me–O bond will lead to an increase of temperature at which the structural fragments of amorphous hydroxide will start to reconstruct leading to their

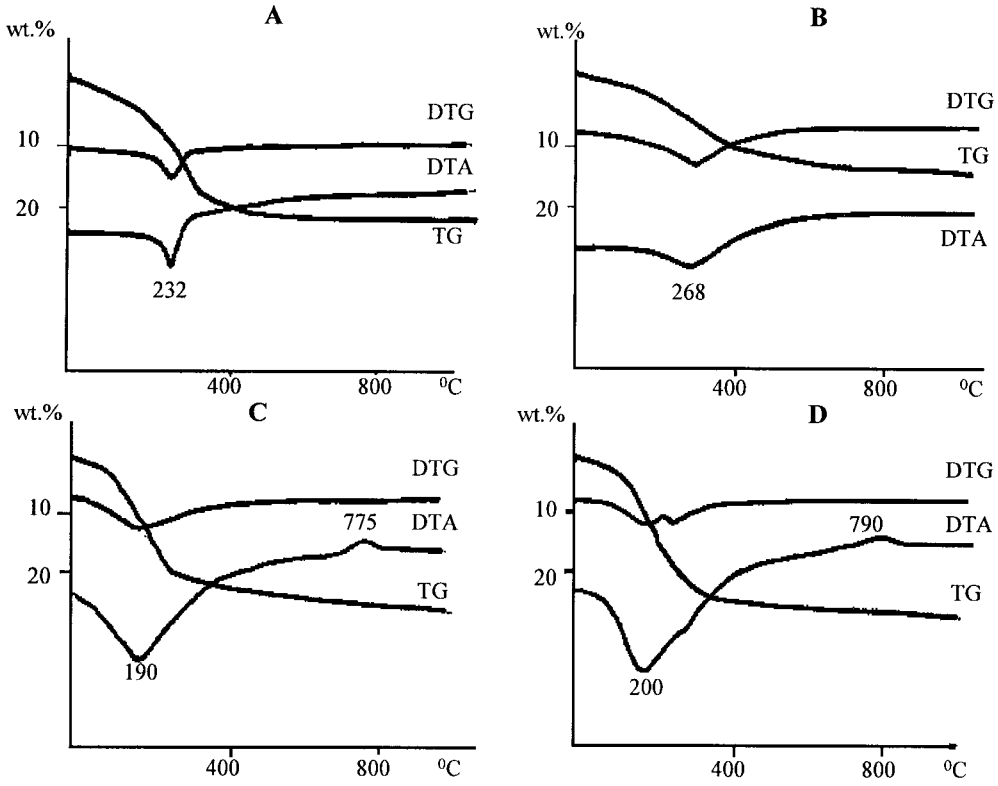

Fig. 1. DTA, DTG and TG curves of In–Ga blended hydroxides: A, 0% Ga_2O_3; B, 20% Ga_2O_3; C, 80% Ga_2O_3; D, 100% Ga_2O_3.

crystallization. At the same time, the opposite picture has been observed for compositions with low content of In component. The crystallization of Ga_2O_3 accelerated with the presence of small quantities of In-dopands which is proved by the lowering of the endorthem temperature caused by formation of α-Ga_2O_3 and as well as by decreasing the exotherm temperature caused by formation of β-Ga_2O_3 for composition with 80 wt% Ga_2O_3.

3.2 XRD investigation

Examination of the precipitates phase composition in the $In(OH)_3$–$Ga(OH)_3$ systems showed that the crystallinity of the precipitates decreases with increasing amounts of Ga-dopants. Thus, diffraction patterns of pure $In(OH)_3$ shows the presence of well crystallized structure while the precipitates with 20 and 40 wt% of Ga-dopants are completely amorphous. Heat-treatment of the precipitates leads to their transformation from hydroxides to the oxides forms. It has been observed that the temperature transition to oxides correlates with the Ga-dopands content. For instance, diffractograms of the precipitates containing 10 wt% Ga_2O_3 showed diffused peaks of In_2O_3 at 600°C whilst samples with 20 and 40 wt% Ga-dopands are still amorphous at this temperature [Fig. 2(a)]; these precipitates transform to oxides at 800°C [Fig. 2(b)]. Samples with 60 and 80 wt% Ga-dopand transform to oxides at over 1000°C. The observed dependence of the amorphous precipitates transition to oxides with the temperature of calcination are well explained by the effect of crystallization retardation [7].

Analysis of the precipitates calcined at 850°C for 2 h showed that the phase composition in all samples is presented by In_2O_3 crystallized in cubic symmetry (Fig. 3). Increase of Ga-dopands leads to decrease in the intensity of In_2O_3 peaks and also their smoothening. At the same time, the presented fragments of diffractograms indicate that an increase of Ga-dopands is accompanied by formation of the other minor phase, traces of which can be seen within the (30–31)2Θ for the sample with 20% Ga_2O_3. Application of the deconvolution technique for analysis of integrated profiles revieled that the phase composition was presented by two phases. The major phase is cubic In_2O_3 seen by two main peaks, (222) and (400) (Fig. 4). The other minor phase was identified as In_2O_3 as well, but crystallized with a rhombohedral type of symmetry. This phase, in the presented fragment, is indicated by two main peaks, (104) and (110) (Fig. 4).

Unit cell refinement of the In_2O_3 structure with Ga-dopands was performed on the basis of assumed cubic symmetry. The sample with 40% Ga_2O_3 was omitted because of the high content of the In-rhombohedral phase and a high degree

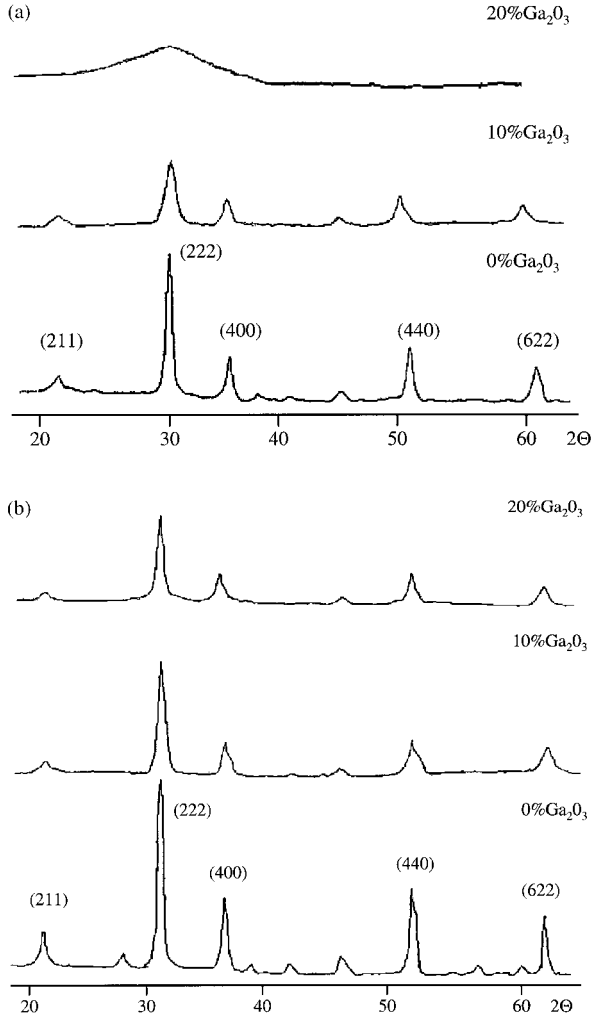

Fig. 2. (a) Diffraction patterns of precipitates calcined at 600°C. (b) Diffraction patterns of precipitates calcined at 800°C.

diffusivity of In_2O_3 peaks. The continuos scans and subsequent crystal structure analysis were performed with an external standard of annealed analytical grade tungsten powders. Peaks accepted for least square refinement of cubic unit cell were selected between 35 up to 90 2Θ. Calculated values of lattice unit cell dimensions with respect to Ga-dopads content are presented in Table 1 and illustrated in Fig. 5.

The above results can lead to the following conclusions. Firstly, the established dependence of lattice parameters of the In_2O_3 unit cell on Ga-dopands content indicates the formation of a limited solid solution in the In_2O_3–Ga_2O_3 system (Fig. 5). The established limit of Ga solubility in C-cubic In_2O_3 phase which lies within 11–12 wt% (15–16·5 mol%) correlates well with data presented in Ref. 8. Secondly, decrease of lattice dimension with increasing Ga-content correlates well with their ionic radii in terms of formation in the system substitution solid solution by substituting of In-ions with high ionic radii (0·79 Å) by smaller Ga-ions (0·62 Å).[9]

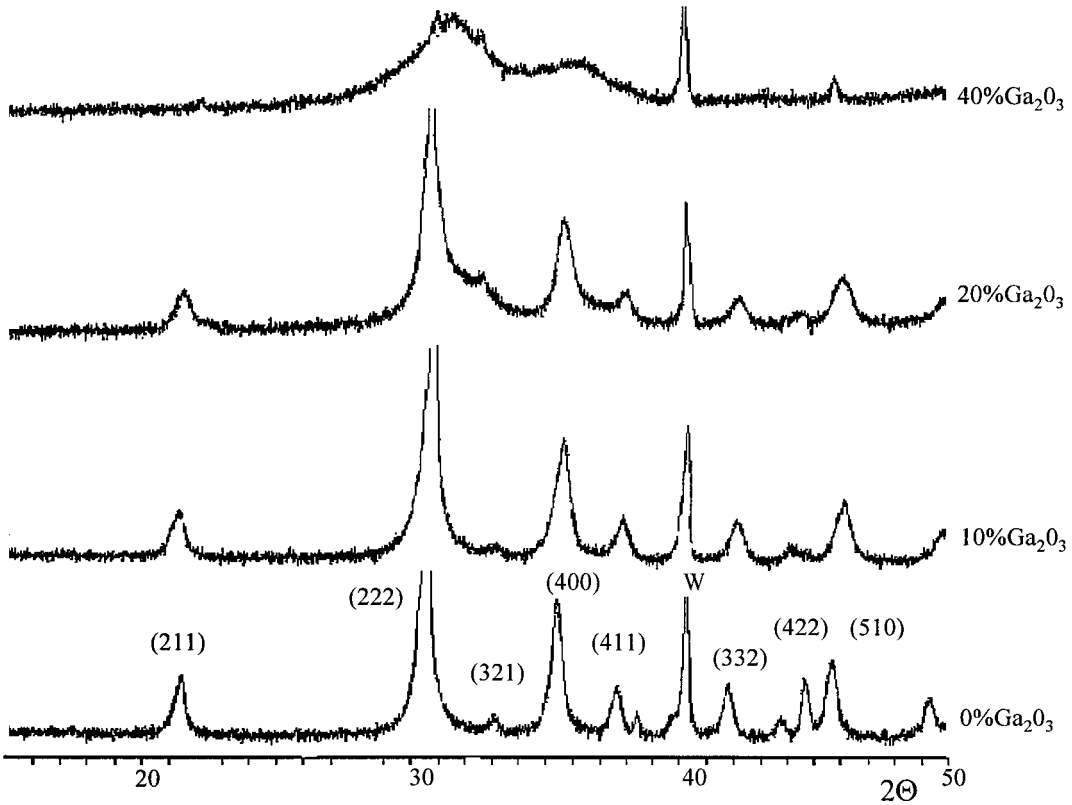

Fig. 3. Diffraction patterns of precipitates calcined at 850°C for 2 h.

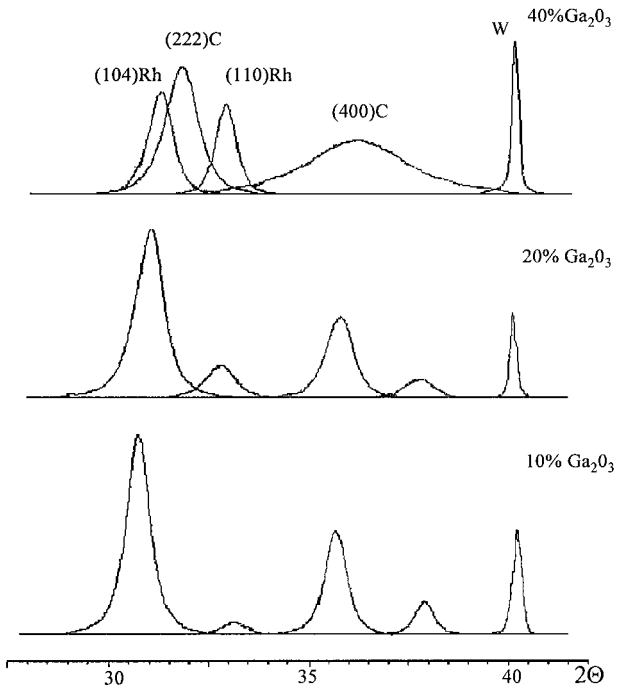

Fig. 4. Fragments of diffraction patterns after deconvolution of the overlapped peaks.

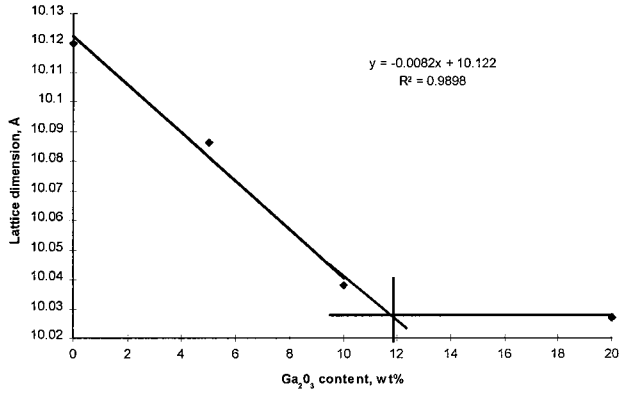

Fig. 5. Lattice parameters of solid-solutions in the In_2O_3–Ga_2O_3 system.

Table 1. Calculated lattice parameters In_2O_3–Ga_2O_3 solid solution

Ga_2O_3 content (wt%)	*Lattice parameter (Å)*
0	$10{\cdot}11977 \pm 0{\cdot}605\times10^{-3}$
5	$10{\cdot}08616 \pm 0{\cdot}207\times10^{-2}$
10	$10{\cdot}03819 \pm 0{\cdot}239\times10^{-2}$
20	$10{\cdot}02734 \pm 0{\cdot}169\times10^{-2}$

3.3 Sorption properties

Data on specific surface area (SSA) and porous sorption volume (V_s) of the precipitates investigated compositions calcined at different temperature are summarised in Table 2. The presented data illustrate that specific surface area and sorption volume are dependent on temperature calcination and phase composition. For instance, increase of Ga-dopands up to 20 wt% causes a maximum increase of a precipitates surface area from $132\,m^2\,g^{-1}$ (0 wt% Ga_2O_3) to $202\ m^2\,g^{-1}$ (20 wt% Ga_2O_3) as well as porosity volume from $0{\cdot}24\,cm^3\,g^{-1}$ to

Table 2. Sorption properties of In_2O_3–Ga_2O_3 precipitates

Content Ga_2O_3	*Parameters*	$T_{calcination}$, °C				
		120	*500*	*700*	*800*	*1000*
0	S_{ssa}, ($m^2\,g^{-1}$)	132	46	45	33	5
	V_s ($cm^3\,g^{-1}$)	0·24	0·26	0·21	0·18	0·03
	D_{pore} (Å)	73	223	178	155	71
5	S_{ssa} ($m^2\,g^{-1}$)	88	50	32	31	7
	V_s ($cm^3\,g^{-1}$)	0·33	0·31	0·23	0·23	0·04
	D_{pore} (Å)	135	273	291	289	65
10	S_{ssa} ($m^2\,g^{-1}$)	128	55	44	40	12
	V_s ($cm^3\,g^{-1}$)	0·35	0·32	0·32	0·26	0·02
	D_{pore} (Å)	104	293	299	278	75
20	S_{ssa} ($m^2\,g^{-1}$)	202	107	96	68	10
	V_s ($cm^3\,g^{-1}$)	0·43	0·34	0·33	0·25	0·02
	D_{pore} (Å)	85	123	136	118	55
40	S_{ssa} ($m^2\,g^{-1}$)	143	84	78	43	16
	V_s ($cm^3\,g^{-1}$)	0·31	0·26	0·18	0·12	0·03
	D_{pore} (Å)	47	107	123	75	71
60	S_{ssa} ($m^2\,g^{-1}$)	129	64	53	28	23
	V_s ($cm^3\,g^{-1}$)	0·28	0·23	0·12	0·05	0·05
	D_{pore} (Å)	31	101	119	77	74
80	S_{ssa} ($m^2\,g^{-1}$)	115	62	48	13	9
	V_s ($cm^3\,g^{-1}$)	0·21	0·23	0·12	0·04	0·03
	D_{pore} (Å)	30	100	112	94	77
100	S_{ssa} ($m^2\,g^{-1}$)	112	58	46	14	12
	V_s ($cm^3\,g^{-1}$)	0·12	0·22	0·12	0·03	0·03
	D_{pore} (Å)	32	104	100	112	102

$0{\cdot}43\,cm^3\,g^{-1}$. Further increase of Ga-dopands leads to a decrease of the specific surface area and porosity volume to minimum values which is, for the pure Ga_2O_3 precipitate, $112\,m^2\,g^{-1}$ and $0{\cdot}12\,cm^3\,g^{-1}$ respectively.

The observed dependence of the specific surface area and porosity volume values of the sedimented precipitates on their composition can be interpreted by the mutual effects of precipitating components at the stage of the formation of the sol structure.[10] From this point, particles of the second component (low concentration of the Ga-dopands) introduced into the developing structure of the first component (indium hydroxides) reduce their growth and lead to the structure becoming disordered by components stacking. As a consequence of this, the precipitates showed an increase of values of both specific surface area and porosity volume.

Analysis of the precipitates surface area and porosity volume in terms of calcination temperature showed a continuous decrease of this parameters which was observed for all compositions and for all temperatures. However, in the presented data, the reduction of V_s and SSA are different for the blended precipitates and for the monophase hydroxides. Thus, after calcination at 800°C the precipitate with 20 wt% Ga-dopand showed maximum residual specific surface area and porosity values of $68\,m^2\,g^{-1}$ and $0{\cdot}25\,cm^3\,g^{-1}$, respectively. For comparison, equivalent parameters for monophase precipitates were $33\,m^2\,g^{-1}$ and $0{\cdot}18\,cm^3\,g^{-1}$ for In_2O_3 and $14\,m^2\,g^{-1}$ and $0{\cdot}03\,cm^3\,g^{-1}$ for Ga_2O_3 (Table 2).

3.4 Electroconductivity measurements

As was pointed out in Ref. 11, the surface of semiconductors containing chemisorbed oxygen atoms can be electrically neutral or negatively charged. Interaction of active gas and semiconductor leads to reactive desorption of physically adsorbed oxygen. As a consequence, free electrons are injected into the conductive zone of the semiconductor varying its elctroconductivity. Based on this concept, an investigation of the electroconductivity of the sintered samples was undertaken at different temperatures in different gases.

Results of the measured specific resistivity of pure In_2O_3 in air at different temperatures (Fig. 6) showed a curve typical for metaloxide semiconductors,[12] particularly, for SnO_2 which is characterized by the existence of a maximum in the curve. The appearance of a maximum resistivity at a given temperature is related to the formation of negatively charged oxygen ions such as O_2^-, O^{2-}, O^- at the oxide surface and as a consequence the resistivity increases. This maximum for In_2O_3 resistivity was observed at 340°C in air but was considerably reduced in a methane-air mixture (Fig. 7).

The gas-sensitivity properties for the obtained solids were estimated through relative resistivity as:

$$R = (\rho_{air} - \rho_{gas})/\rho^*_{air}100\%,$$

where ρ_{air} is the specific resistivity in air; ρ_{gas} is the specific resistivity in gas. From Fig. 8, for a concentration of 0·5 vol% methane in air, the relative resistivity can be estimated to be equal 40%. It should be noted that the maximum sensitivity to

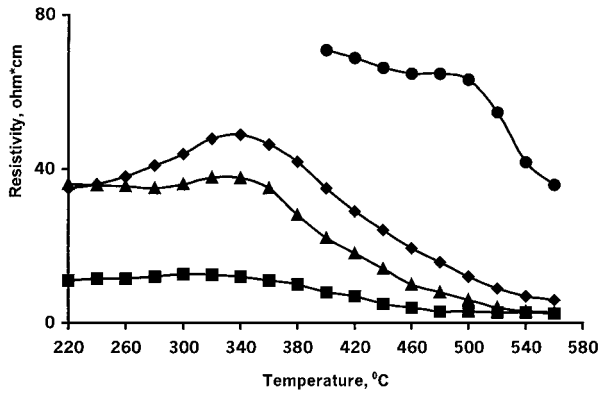

Fig. 6. Resistivity versus temperature in air: In_2O_3(◆); In_2O_3 + 5 wt% Ga_2O_3(■); In_2O_3 + 10 wt% Ga_2O_3(▲); In_2O_3 + 20 wt% Ga_2O_3(●).

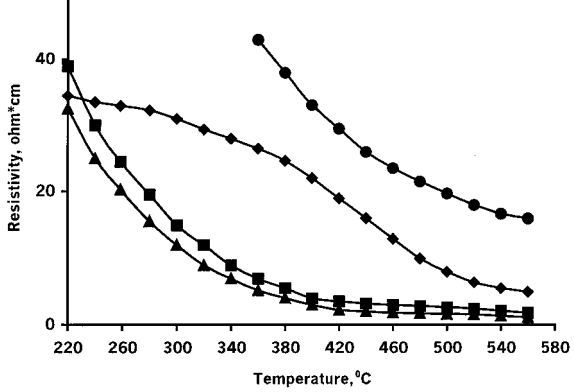

Fig. 7. Resistivity versus temperature in air blended with 0·5 vol% CH_4: In_2O_3(◆); $In_2O_3 + 5$ wt% Ga_2O_3(■); Where $In_2O_3 + 10$ wt% Ga_2O_3(▲); $In_2O_3 + 20$ wt% Ga_2O_3(●).

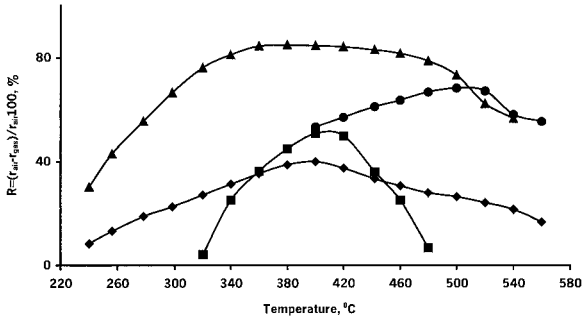

Fig. 8. Relative resistivity versus temperature in air blended with 0·5 vol% CH_4: In_2O_3(◆); $In_2O_3 + 5$ wt% Ga_2O_3(■); $In_2O_3 + 10$ wt% Ga_2O_3(▲); $In_2O_3 + 20$ wt% Ga_2O_3(●).

methane gas was observed at 400°C. This indicates a high probability that the high temperature forms oxygen, O^-, affects the methane oxidation. Also from Fig. 8, an increase of Ga-dopands lead to the shift of the maximum sensitivity to methane gas from 400°C (0% Ga_2O_3) to 520°C (20% Ga_2O_3). The other interesting feature is that the sample with 10% Ga_2O_3 showed a constant R value within a wide temperature interval from 340 to 480°C.

In fact, the maximum sensitivity of a semiconductive gas sensor can be released as a rule in a diffusion field of interaction between the moleculs of detected gas and active oxygen forms at the ceramic surface.[13] As a consequence, the increased gas sensitivity of modified In_2O_3 (10% Ga_2O_3) ceramic with respect to undoped In_2O_3 can be explained by leading role of diffusion processes and, respectively by the oxides structure in terms of median porous sizes (d_{pore}) or distribution of their volume as takes place in the case of thermocatalytic sensors.[14] In the present work, this dependence of relative electrical resistively on average (median) pore size has been demonstrated.

4 Conclusion

The presented experimental data demonstrated that solubility of Ga_2O_3 in In_2O_3 cubic lattice has a limit up to 11–12 wt%. Examination of the structure and sorption properties showed that solids obtained by the coprecipitation route has a linear dependence of crystallization path and porosity volume of calcined solids on the concentration of Ga_2O_3-dopands. It has been demonstrated that the formation of the porous structure of In_2O_3 ceramics doped with Ga_2O_3 was a key factor leading to high sensitivity of the modified ceramics. Ceramics materials for application as an n-active element in semiconductive gas sensors with composition In_2O_3–Ga_2O_3 (10 wt%) was selected.

References

1. Morrison, S. R., New materials in sensor technology. 2. In *International Meeting on Chemical Sensors*, eds J.-L. Acoutourier *et al.* Bordeaux, 7–10 July, 1986, D.39–41.
2. Trofimenko, N. E., Komarov, V. S., Baran, S. V. and Ratko, A. I., Sorption and gas sensitive properties of In_2O_3 based ceramics doped by Al_2O_3. *Journal of Physical Chemistry*, 1995, **69**(5), 910–914.
3. Fleischer, M. and Meixner, H. B., Gallium oxide thin films: a new material for high-temperature oxygen sensors. *Sensors and Actuators B*, 1990, **1**, 437–441.
4. Fleischer, M. and Meixner, H. B., A selective CH_4 sensors using semiconducting Ga_2O_3 thin films based on temperature switching of multigas reaction. *Sensors and Actuators B*, 1995, **25**, 544–547.
5. Kovtonuk, N. F. and Kontsevoj, J. A., Measurements parameters of semiconductors. *Metallurgy (Moscow)*, 1970, 432.
6. Reznitskij, L. A. and Fillipova, C. E., Crystallization inhibitors of amorphous substance. *Progress in Chemistry*, 1993, **62**(15), 474–485.
7. Ivanova, A. S., Dzisko, V. A. and Ketchic, S. V., Influence of the method of making solid phases in the system MgO–Al_2O_3–H_2O on their properties. *Journal of Inorganic Chemistry*, 1980, **25**(9), 23–30.
8. Schneider, S. J., Roth, R. S. and Waring, J. L., Solid state reactions involving oxides of trivalent cations. *J. Res. Natl. Bur. Stand.*, 1961, **65A**, 345–374.
9. Shannon, R. D. and Prewitt, C. T., Effective ionic radii in oxides and fluorides. *Acta Crystallogr.*, 1969, **B25**, 925.
10. Dzisko, B. A., *Basis of Methods of Catalyst Preparations*. Nayka, Novosibirsk, Russia, 1983, pp. 46–48.
11. Volkenhtain, F. F., *Electron Process at the Surface of Semiconductors at Chemisorption*. Nayka, Moscow, Russia, 1987, pp. 93–95.
12. Schierbaum, K. D., Geiger, J., Weiman, U. and Gopel, W., Specific palladium and platinum doping for tin oxide-based thin film sensor arrays. *Sensors and Actuators B*, 1993, **13/14**, 143–147.
13. Gentry, S. and Jones, A., Poisoning and inhibitor of catalytic oxydation. *J. Appl. Chem. Biotechnol.*, 1978, **28**, 727–731.
14. Baran, S. V., Trofimenko, N. E., Komarov, V. S. and Ratko, A., Influence of a carrier porous structure on properties of thermocatalytic sensors. *Vesti AN Belarus, ser. Chim. Nayk*, 1992, **5–6**, 25–28.